

Typical altermagnetism with huge nonrelativistic spin-split and flat band in the bulk CoF_2

Bo-Wen Yu and Bang-Gui Liu*

*Beijing National Laboratory for Condensed Matter Physics,
Institute of Physics, Chinese Academy of Sciences, Beijing 100190, China and
School of Physical Sciences, University of Chinese Academy of Sciences, Beijing 100049, China*
(Dated: November 26, 2024)

Recently, a third phase named altermagnet, has been introduced to describe a special magnetic state and some materials are classified as altermagnets. Here, our first principles calculations indicate that the bulk CoF_2 is an altermagnet with a huge spin-split and flat bands near the Fermi energy. By comparing the results with and without spin-orbit coupling, it can be shown that the huge spin splitting is not caused by relativistic effects but rather by a special symmetry. There are also flat bands near the Fermi energy which can be adjusted by changing the direction of the magnetic moment. From the band structure, we obtain a spin-resolved effective low-energy model that describes a quasi-two-dimensional hole gas with two independent spin components, leading to exotic transport phenomena that are distinct from those in conventional two-dimensional or bulk materials. Therefore, the bulk CoF_2 is a typical altermagnet with a huge nonrelativistic spin-split and flat bands which deserves further study for the potential spintronics and electronics applications.

I. INTRODUCTION

As the most fundamental field in physics and materials science and traditional, magnetism divides magnetic material into two phases that are known as the ferromagnets and antiferromagnets. Recently a new phase named altermagnet [1, 2] is introduced to describe a special magnetic state, which is seen as a breakthrough in the field of fundamental magnetism during the past few years. This new phase of magnetism is being re-understood theoretically and experimentally[3–20]. Many conventional antiferromagnets, such as RuO_2 [21–35], CaCrO_3 [36], FeF_2 [37], MnF_2 [23, 38], MnO_2 [39, 40], LaMnO_3 [41, 42], CrSb [2, 43, 44], $\text{Fe}_2\text{Se}_2\text{O}$ [45], RuF_4 [46], MoTe [47], $\alpha\text{-MnTe}$ [48–51] and MnTe_2 [52–54] can be classified as altermagnetic materials[55]. Further research and more altermagnetic material candidates are expected in order to seek more phenomena and potential applications for electronics, spintronics and multiferroics.

The fundamental properties of CoF_2 , which is famous as an antiferromagnetic wide bandgap semiconductor have been studied theoretically and experimentally[56–62]. Previous study about the piezomagnetic effect show the potential applications of CoF_2 in emerging spintronics[61]. However, the RuO_2 [21–31] which is famous for its nonrelativistic collinear antiferromagnetism and spin-split[31, 63–66] has similar rutile structures with CoF_2 . Nonrelativistic spin-momentum coupling may cause spin-polarized current under an external electric field or temperature gradient [21, 36, 67, 68], which is called the spin-splitter effect[63].

Here, we study on the electronic structure of the bulk CoF_2 through the first-principles calculations and confirm that there is huge spin-split near the Fermi energy

which can provide evidence to divide CoF_2 into altermagnets. Further analysis of atom-projected band structures and the results of the comparison of the calculation with spin-orbit coupling(SOC) and without SOC show that the spin-split is a nonrelativistic effect and caused by the special symmetry of CoF_2 lattice. We also find the flat bands near the Fermi energy and get the spin-resolved effective low-energy model. The flat bands may make holes near the band edge behave like those in two-dimensional(2D) materials. Furthermore, we study the spin transport properties by effective model and investigate the topology properties under the external electric and magnetic fields. Computational methods and more detailed results will be presented in the following.

II. METHODOLOGY

The first-principles calculations are performed with the projector-augmented wave (PAW) method within the density functional theory[41], implemented in the Vienna Ab-initio simulation package software (VASP) [69]. The generalized gradient approximation (GGA) revised for solids by Perdew, Burke, and Ernzerhof (PBEsol)[70, 71] is used as the exchange-correlation functional. The self-consistent calculations are carried out with a Γ -centered ($12 \times 12 \times 19$) Monkhorst-Pack grid[72]. The kinetic energy cutoff of the plane wave is set to 450 eV. The convergence criteria of the total energy and force are set to 10^{-7} eV and 0.001 eV/Å. The spin-orbit coupling (SOC) is applied in the calculation of band structure and magnetocrystalline anisotropy energy. The Hubbard-U term [73] is considered to improve energy band description.

* bgliu@iphy.ac.cn

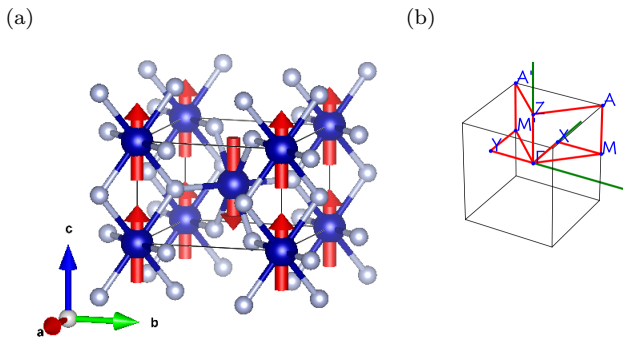


FIG. 1: (a)The structures of CoF_2 . The Co atom is located at the center of an octahedral composed of six F atoms. Arrows indicate spin conditions at the lowest energy for the altermagnetic phase. (b)Brillouin zone of CoF_2 .

III. RESULT AND DISCUSSION

The structure and basic properties of the bulk CoF_2 have been studied theoretically and experimentally. It is reported that there are several materials[21–23, 36–39, 74] can be recognized as altermagnets with similar rutile structures. The structure of CoF_2 is presented in FIG. 1. Both the theoretical work and the X-ray diffraction experiments show that CoF_2 has a rutile structure, space group $D144h$. The lattice constant of bulk CoF_2 is experimentally measured to be $a = 4.695 \text{ \AA}$ and $c = 3.180 \text{ \AA}$ [56]. And the equilibrium lattice constants calculated by structural optimization is $a = 4.646 \text{ \AA}$ and $c = 3.157 \text{ \AA}$ which is reasonable considering the error of the calculation. There are 6 atoms in the lattice of bulk CoF_2 . The two Co atoms are located at $(0,0,0)$ and $(0.5,0.5,0.5)$ with magnetic moment of $3.000 \mu_B$ and $-3.000 \mu_B$, which cancel each other out and the total magnetic moment of the unit cell is zero. Therefore the two Co atoms and their neighboring F atoms can be divided into two sublattices. In terms of symmetry, the two sublattices can be transformed into each other through a twofold spin-space rotation with a fourfold real-space rotation and a translation operation[55, 75, 76]. It is the F atoms around each Co atom and the octahedral environment with tetragonal symmetry that destroy the time-reversal symmetry, which results in huge anisotropic nonrelativistic spin-split.

There are 9 electrons in the 3d and 4s orbitals of the Co atom and there are 3 single d electrons per Co atom left after bonding with the +2 valence in the CoF_2 . In order to confirm the direction of the easy axis, we calculate the total energies along different directions. The results show that the state that magnetic moment is oriented in the [001] direction has the lowest total energy and the total energy difference between the other direction and ground state is 0.0002eV for [100] and 0.0012eV for [110].

The main electric structure is shown in FIG. 2. Sev-

eral methods which include HSE06[77], PBE+U and PBEsol+U are used for a comprehensive evaluation of the band structure. The results of different methods are presented in FIG. S1(supplemental materials). Considering the gap calculated by HSE06 is generally larger than the real situation, $U=3\text{eV}$ may be the best value. The gap of CoF_2 is 2.5 eV and which indicates that CoF_2 is a kind of wide bandgap semiconductors. The spin-resolved band structure without SOC show that the CBM is at point A in the Brillouin zone for both spin up and down and VBM is at the line Γ to M $(0.5,0.5,0)$ for spin up and the line Γ to M' $(-0.5,0.5,0)$ for spin down. The presence of spin splitting in both the results without and with SOC confirms that this spin splitting does not come from SOC. Nonrelativistic spin-split mainly occurs along the line M' to M, which is also the diagonal of the Brillouin zone. The spin up band becomes a flat band near the Fermi energy and the spin down band stays away from Fermi energy along the line Γ to M, while the spin down band becomes flat band near the Fermi energy and the spin up band stays away from Fermi energy along the line M' to Γ . The flat bands near the Fermi energy means the holes have a huge effective mass and can hardly move in that direction. The electronic structures of the CoF_2 with the magnetic moment orienting in the [100], [110], and [001] directions are also calculated and the results is demonstrated in FIG. 3. The flat bands will be destroyed and the VBM changed to Γ when the direction of magnetic moment changes. Therefore the properties of the energy band edge can be controlled by adjusting the direction of the magnetic moment.

In order to analyze the relationship between the spin and different Co atoms and find the reason of the huge spin split, the band structure with atom and orbital projections for the two Co atoms is shown in Fig. S2(supplemental materials). There are only 7 electrons occupying the 5 3d orbitals and each of the five 3d orbitals owns an electrons at 1.5eV below the Fermi energy. For the electrons near the Fermi energy, the linear combination of d_{xz} and d_{yz} with equal weights owns one electron, which is located in the first band under the Fermi energy for the single spin channel. The last electron is located in a linear combination of d_{xy} and d_{z^2} (d_{z^2} weights more). It also shows that electrons with the different spin in conduction and valence band is from different Co atoms. The spin up electrons and holes are mainly provided by one Co atom located at $(0.5,0.5,0.5)$, and the spin down electrons and holes are mainly provided by another Co atom located at $(0,0,0)$. This comfire that the huge spin-split is from the special symmetry of the two sublattices in CoF_2 .

Special band structure causes electrons to exhibit special properties, especially in the external electric and magnetic field. The flat band makes holes in the flat band behave like hole gases in two-dimensional materials in some cases. For convenience, the defition of the axis need to be reset. The xyz axes are perpendicular to each other. The z axis is along the c direction of the lattice,

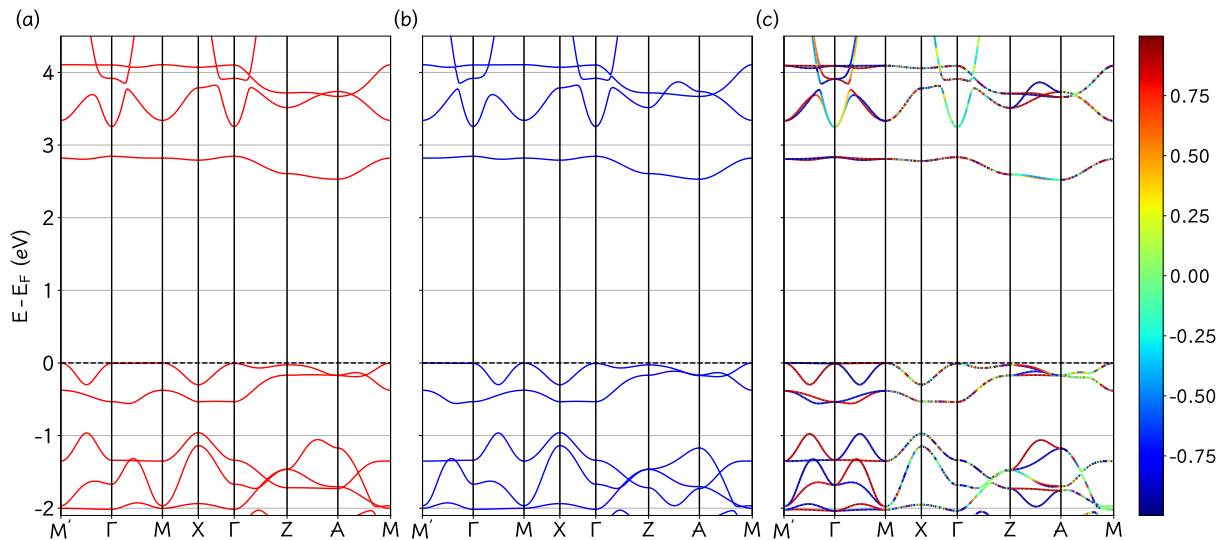


FIG. 2: The band structures((a)(b) for the two spin outwith SOC and (c) for without SOC) of CoF₂. The color bar describes the electronic spin polarization with SOC, where ± 1 corresponds to the two 100% spin polarizations.

x and y axis are along the diagonal of the Brillouin zero. The schematic diagram of the direction of x and y axis is shown in FIG. 4 (a). From the band structure from the first principles calculation, we get a spin-resolved effective low-energy model for valence band. The Hamiltonian of the model for spin up and spin down under external magnetic $B(B_x, B_y, B_z)$ field can be written as

$$\begin{aligned} H_{\uparrow} &= \frac{(\hat{p}_x - q\hat{A}_x)^2}{2M_0} + \frac{(\hat{p}_z - q\hat{A}_z)^2}{2M_z} + \mu|B| \\ H_{\downarrow} &= \frac{(\hat{p}_y - q\hat{A}_y)^2}{2M_0} + \frac{(\hat{p}_z - q\hat{A}_z)^2}{2M_z} - \mu|B| \end{aligned} \quad (1)$$

where M_0 is the effective mass of the hole along the x axis for spin up (y axis for spin down) and M_z is the effective mass along the z axis. The M_0 and M_z can be obtained by fitting the curve of band structure at the conduction band edge. The M_0 is $0.1603 m_e$ and M_z is $0.2461 m_e$ at the M point in Brillouin zone where m_e is the electron mass. The behavior of different spin be studied separately because there is almost no coupling between them. This Hamiltonian describe two independent quasi-2D holes gas along two perpendicular directions. So the gauge of magnetic vector potential $\mathbf{A}(A_x, A_y, A_z)$ can be selected as $\mathbf{A}_{\uparrow} = (0, zB_x - xB_z, -xB_y)$ for spin up and $\mathbf{A}_{\downarrow} = (zB_y - yB_z, 0, yB_x)$ for spin down. Then the Hamiltonian can be written as

$$\begin{aligned} H_{\uparrow} &= \frac{\hat{p}_x^2}{2M_0} + \frac{q^2 B_y^2}{2M_z} \left(\hat{x} - \frac{\hat{p}_z}{qB_y} \right)^2 + \mu|B| \\ H_{\downarrow} &= \frac{\hat{p}_y^2}{2M_0} + \frac{q^2 B_x^2}{2M_z} \left(\hat{y} - \frac{\hat{p}_z}{qB_x} \right)^2 - \mu|B| \end{aligned} \quad (2)$$

So the Hamiltonian of two spin becomes a standard oscillator Hamiltonian and the essential parameters of

the Landau level are $\omega_{\uparrow, \downarrow} = \frac{|qB_{y,x}|}{\sqrt{M_z M_0}}$. The energy for spin up and down is $E_{m, \uparrow} = \hbar\omega_{\uparrow}(m + \frac{1}{2}) + \mu|B|$, $E_{m, \downarrow} = \hbar\omega_{\downarrow}(m + \frac{1}{2}) - \mu|B|$, where m is the number of the Landau level. The formula indicates that the energy level for different spin is related to the direction and strength of the magnetic field. The FIG. 4 (b) show the Landau level with different direction of magnetic field. In this case, the magnetic field is parallel to plane of x and y axis. For θ is $\frac{\pi}{4}$, the magnetic field affects both spins equally, so their Landau level difference is also the same. But there are still energy split between the two spin because of the Zeeman effect. For θ is 0 or $\frac{\pi}{2}$, the magnetic field is perpendicular to the one spin of plane of 2D hole gas and there will be only one set of Landau level of another spin. The energy difference of Landau level depends on the parameters ω and the trend of ω changing with the magnetic field direction is shown in FIG. 4 (c). The strict derivation proof of turning a non-periodic model of the standard two hole or electron gas into a periodic Bloch form and the Chern numbers has been obtained in Ref.[78].

When all r Landau bands are occupied, the Berry curvature for two spin is $\Omega_{xz}(k_x, k_z) = -\frac{r}{qB_y}$ for spin up and $\Omega_{yz}(k_y, k_z) = -\frac{r}{qB_x}$ for spin down. And the Chern numbers are

$$\begin{aligned} \mathcal{C} &= -r \text{sign}(qB_y) \quad (\text{spin up}) \\ \mathcal{C} &= -r \text{sign}(qB_x) \quad (\text{spin down}) \end{aligned} \quad (3)$$

When the external magnetic field with magnitude $|B|$ is perpendicular to the z axis and the angle between the magnetic field and the x axis is θ , the Berry curvature for two spin is $\Omega_{xz, \uparrow}(k_x, k_z) = -\frac{r_{\uparrow}}{|qB| \sin \theta}$ and $\Omega_{yz, \downarrow}(k_y, k_z) = -\frac{r_{\downarrow}}{|qB| \cos \theta}$. The Chern numbers become

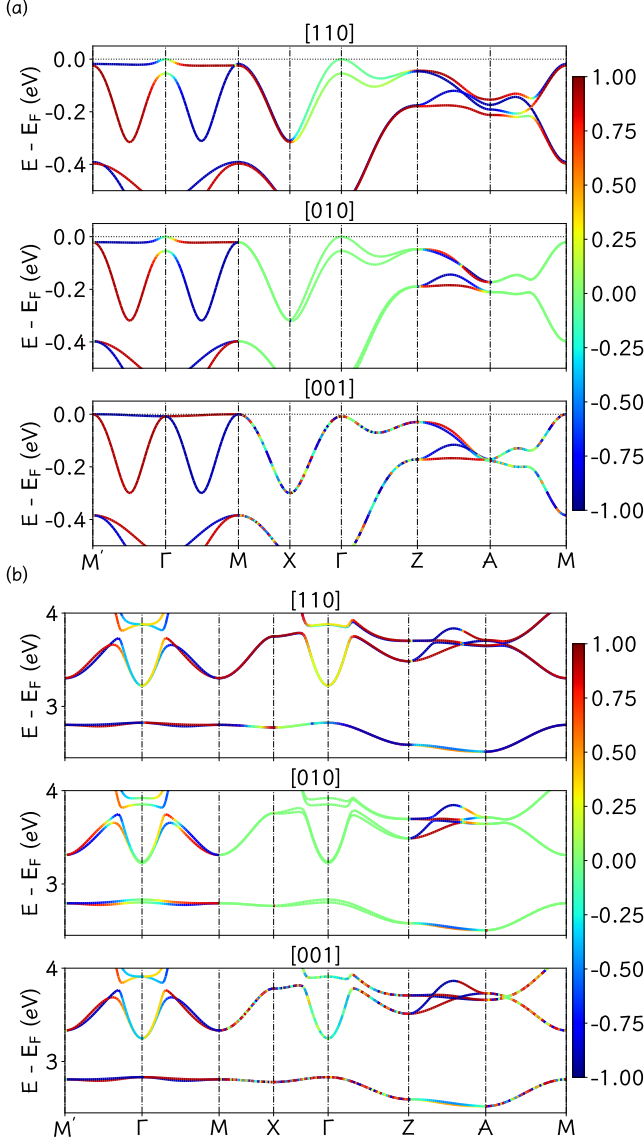


FIG. 3: The electric structures of the CoF₂ with the magnetic moment orienting in the [100], [110], and [001] directions. (a) for conduction band and (b) for valence band. The color bar describes the electronic spin polarization, where ± 1 corresponds to the two 100% spin polarizations.

$-r_{\uparrow} \text{sign}(\sin \theta)$ for spin up and $-r_{\downarrow} \text{sign}(\cos \theta)$ for spin down. The Chern numbers per occupied bands for the two spin with different angle θ are shown in FIG. 4 (d).

For external electric field, it is supposed that the electric field $\mathbf{E}(E_x, E_y, E_z)$ is weak enough that there is little change in the band structure and the crystal structure. According to the the relaxation time approximation, the Boltzmann equation of the distribution function f can be expressed as $\frac{f_k^0 - f_k}{\tau} = \frac{\partial f_k}{\partial t} = \frac{\partial f_k}{\partial E_k} \frac{\partial E_k}{\partial t} = \frac{\partial f_k}{\partial E_k} v_k \cdot \mathbf{E}q$, where τ is the electron relaxation time and $v_k = \frac{d\omega}{dk} = \frac{1}{\hbar} \frac{dE(k)}{dk}$. The longitudinal conductivity[79] with the density of car-

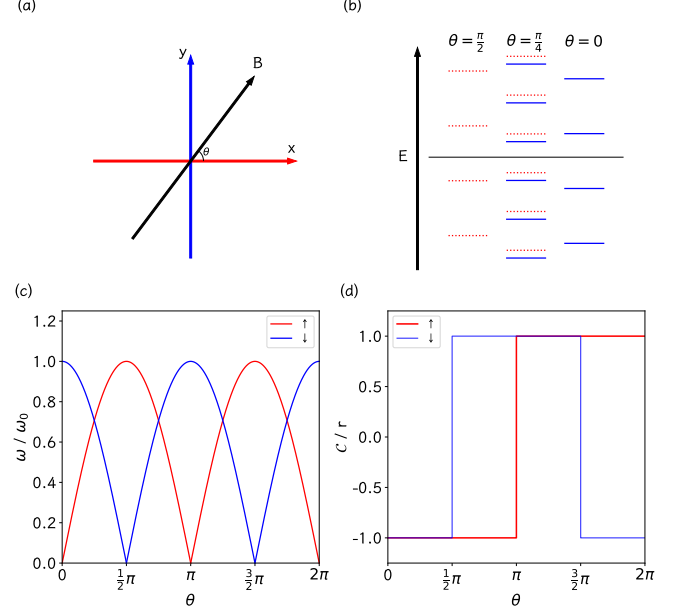


FIG. 4: (a) the definition of the direction of external magnetic field and the 2D hole gas for the two spin. The x (red axis) is for the spin up and the y (blue axis) for the spin down. The angle between the magnetic field and the x axis is θ . (b) the figure for Landau level for the two spin when the angle θ is $0, \frac{\pi}{4}$ and $\frac{\pi}{2}$. (c) the parameter ω for the Landau level for the two spin with different angle θ , where ω_0 is $\frac{|qB|}{\sqrt{M_z M_0}}$. (d) the Chern numbers per occupied bands for the two spin with different angle θ .

riers n can be written as

$$\begin{aligned} \sigma_{xx}^{\uparrow} &= \frac{q^2 \tau n}{M_0} \\ \sigma_{yy}^{\uparrow} &= 0 \\ \sigma_{zz}^{\uparrow} &= \frac{q^2 \tau n}{M_z} \end{aligned} \quad (4)$$

$$\begin{aligned} \sigma_{xx}^{\downarrow} &= 0 \\ \sigma_{yy}^{\downarrow} &= \frac{q^2 \tau n}{M_0} \\ \sigma_{zz}^{\downarrow} &= \frac{q^2 \tau n}{M_z} \end{aligned} \quad (5)$$

The longitudinal conductivity is highly related to the spin and direction. For external electric field along the z axis, the longitudinal conductivity is the same for the two spin and there are both two spin carriers in the no polarized current. But for the external electric field along plane of x and y axis, the longitudinal current is different for the two spin. The current density under the external electric field \mathbf{E} for both spin can be written as

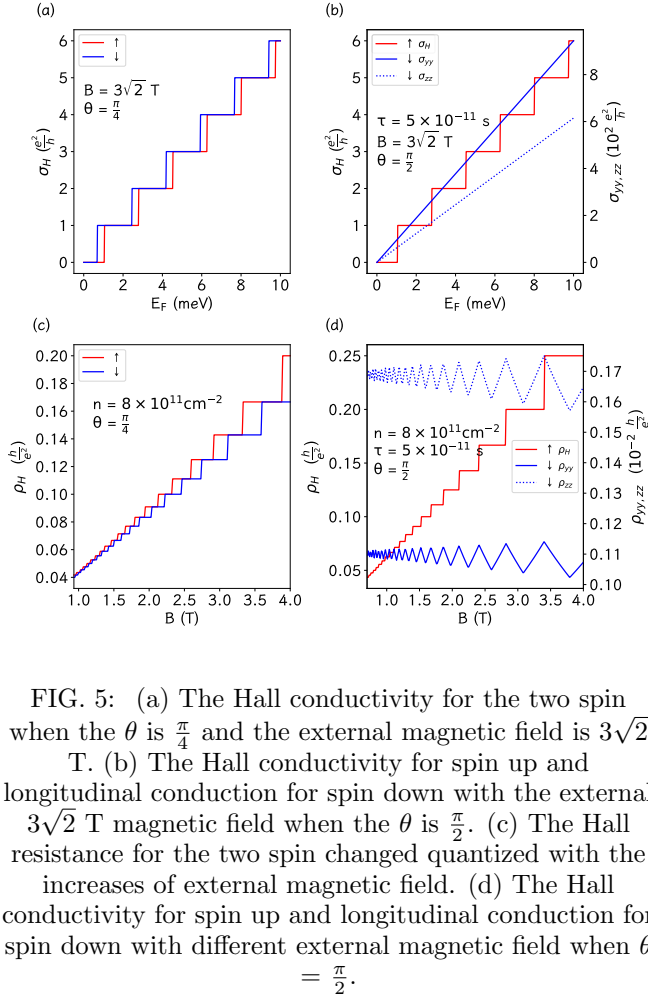


FIG. 5: (a) The Hall conductivity for the two spin when the θ is $\frac{\pi}{4}$ and the external magnetic field is $3\sqrt{2}$ T. (b) The Hall conductivity for spin up and longitudinal conduction for spin down with the external $3\sqrt{2}$ T magnetic field when the θ is $\frac{\pi}{2}$. (c) The Hall resistance for the two spin changed quantized with the increases of external magnetic field. (d) The Hall conductivity for spin up and longitudinal conduction for spin down with different external magnetic field when $\theta = \frac{\pi}{2}$.

$$\begin{aligned} j^\uparrow &= |E| \cos^2 \theta \sigma_{xx}^\uparrow \\ j^\downarrow &= |E| \sin^2 \theta \sigma_{yy}^\downarrow \end{aligned} \quad (6)$$

where θ is the angle between the external electric field and the x axis, $|E|$ is the magnitude of the external electric field. The polarizability of the current is $\frac{j^\uparrow - j^\downarrow}{j^\uparrow + j^\downarrow} = \cos(2\theta)$, which indicates that the polarizability of the current can be changed by the direction of the external electric field. Therefore, there still is pure spin current along the direction which is perpendicular to the external electric field.

$$\begin{aligned} j_s &= |E| \cos \theta \sin \theta \sigma_{xx}^\uparrow + |E| \sin \theta \cos \theta \sigma_{yy}^\downarrow \\ &= |E| \sin(2\theta) \frac{q^2 \tau n}{M_0} \end{aligned} \quad (7)$$

We also find the some special transport phenomena which is different from the traditional 2D or bulk systems. The Hall conductivity(resistance) under the external magnetic field can be obtained by the previous Chern number and the longitudinal conductivity(resistance) can

be exported from the relaxation time approximation. For the special situation where θ is $\frac{\pi}{4}$ and θ is $\frac{\pi}{2}$, the resistance is calculated when the density of carriers is $8 \times 10^{11} \text{ cm}^{-2}$ and the relaxation time is $5 \times 10^{-11} \text{ s}$. The results is shown in FIG. 5. For θ is $\frac{\pi}{4}$, the effect magnetic field applied to spin up and down is the same. The Hall conductivity and Hall resistance are shown in FIG. 5(a)(c). The carriers of both two spin can form the Landau level with the same energy level difference independently. Their Hall conductivity changed quantized with the increases of Fermi level and their Hall resistance increases quantized as the external magnetic field increases. However the Zeeman item in their Hamiltonian cause the energy level split and their Landau level change asynchronously with the external magnetic field increases because the carriers are shared by the two spin and the lowest energy level is always occupied first. For θ is $\frac{\pi}{2}$ (shown in FIG. 5(b)(d)), the external magnetic field is perpendicular to the y axis and only the spin up can form the Landau level. The behavior of spin down is similar to that of an anisotropic two-dimensional free particle system. So the Hall conductance for spin up increases quantized and the longitudinal conduction for spin down increases linearly as raise of Fermi level. Same as the previous case, carriers are also shared by the two spin which caused the Hall resistance increases quantized as the external magnetic field increases for spin up and the longitudinal resistance of spin down oscillates periodically as the external magnetic field increases.

IV. CONCLUSION

In summary, we believe that CoF_2 can be classified as altermagnet according to the results of first-principles calculation. The special symmetry and sublattices of rutile structure make CoF_2 become altermagnetic material. The band structure shows that there is a huge anisotropic spin-split and a flat band near the Fermi level. The comparison of the calculation with SOC and without SOC indicates that the spin-split is a nonrelativistic effect. Further analysis for the atoms and orbitals projections shows that the bands with different spin are from different Co atoms near the Fermi level. The anisotropy of the spin-split is from the octahedral environment with tetragonal symmetry, which is constituted by F atoms around each Co atom. We also find the flat bands near the Fermi level and get a spin-resolved effective low-energy model. The flat bands near the Fermi level can be destroyed by changing the direction of the magnetic moment, which provides a potential method to control the properties of band edge. We investigate the transport properties under the external electric and magnetic fields and find quantum Hall effect and spin-splitter effect. The features of quasi-2D holes gas and the strong coupling between spin and direction make it postible to control the spin composition by changing the direction of the external electric field, which provides a potential research value for

the spintronics and electronics applications. The special properties of the bulk CoF_2 can make it interested to seek the new properties and potential applications of CoF_2 or other similar altermagnets.

ACKNOWLEDGMENTS

This work is supported by the Strategic Priority Research Program of the Chinese Academy of Sciences (Grant No. XDB33020100) and the Nature Science Foundation of China (Grant No.11974393). All the numerical calculations were performed in the Milky Way #2 Supercomputer system at the National Supercomputer Center of Guangzhou, Guangzhou, China.

-
- [1] I. Mazin (The PRX Editors), *Phys. Rev. X* **12**, 040002 (2022).
- [2] L. Šmejkal, J. Sinova, and T. Jungwirth, *Phys. Rev. X* **12**, 031042 (2022).
- [3] Z. Xiao, J. Zhao, Y. Li, R. Shindou, and Z.-D. Song, *Phys. Rev. X* **14**, 031037 (2024).
- [4] X. Chen, J. Ren, Y. Zhu, Y. Yu, A. Zhang, P. Liu, J. Li, Y. Liu, C. Li, and Q. Liu, *Phys. Rev. X* **14**, 031038 (2024).
- [5] Y. Jiang, Z. Song, T. Zhu, Z. Fang, H. Weng, Z.-X. Liu, J. Yang, and C. Fang, *Phys. Rev. X* **14**, 031039 (2024).
- [6] S. F. Weber, A. Urru, S. Bhowal, C. Ederer, and N. A. Spaldin, *Phys. Rev. X* **14**, 021033 (2024).
- [7] J. A. Ouassou, A. Brataas, and J. Linder, *Phys. Rev. Lett.* **131**, 076003 (2023).
- [8] S. A. A. Ghorashi, T. L. Hughes, and J. Cano, *Phys. Rev. Lett.* **133**, 106601 (2024).
- [9] Y. Fang, J. Cano, and S. A. A. Ghorashi, *Phys. Rev. Lett.* **133**, 106701 (2024).
- [10] T. Sato, S. Haddad, I. C. Fulga, F. F. Assaad, and J. van den Brink, *Phys. Rev. Lett.* **133**, 086503 (2024).
- [11] R.-W. Zhang, C. Cui, R. Li, J. Duan, L. Li, Z.-M. Yu, and Y. Yao, *Phys. Rev. Lett.* **133**, 056401 (2024).
- [12] P. Das, V. Leeb, J. Knolle, and M. Knap, *Phys. Rev. Lett.* **132**, 263402 (2024).
- [13] V. Leeb, A. Mook, L. Šmejkal, and J. Knolle, *Phys. Rev. Lett.* **132**, 236701 (2024).
- [14] P. A. McClarty and J. G. Rau, *Phys. Rev. Lett.* **132**, 176702 (2024).
- [15] S. Bhowal and N. A. Spaldin, *Phys. Rev. X* **14**, 011019 (2024).
- [16] H. Bai, Y. C. Zhang, Y. J. Zhou, P. Chen, C. H. Wan, L. Han, W. X. Zhu, S. X. Liang, Y. C. Su, X. F. Han, F. Pan, and C. Song, *Phys. Rev. Lett.* **130**, 216701 (2023).
- [17] D. Chakraborty and A. M. Black-Schaffer, *Phys. Rev. B* **110**, L060508 (2024).
- [18] S. Banerjee and M. S. Scheurer, *Phys. Rev. B* **110**, 024503 (2024).
- [19] S.-B. Zhang, L.-H. Hu, and T. Neupert, *Nature Communications* **15**, 1801 (2024).
- [20] H. Reichlova, R. Lopes Seeger, R. González-Hernández, I. Kounta, R. Schlitz, D. Kriegner, P. Ritzinger, M. Lammel, M. Leiviskä, A. Birk Hellenes, K. Olejník, V. Petříček, P. Doležal, L. Horak, E. Schmoranzero, A. Badura, S. Bertaina, A. Thomas, V. Baltz, L. Michez, J. Sinova, S. T. B. Goennenwein, T. Jungwirth, and L. Šmejkal, *Nature Communications* **15**, 4961 (2024).
- [21] L. Šmejkal, R. González-Hernández, T. Jungwirth, and J. Sinova, *Science Advances* **6**, eaaz8809 (2020).
- [22] K.-H. Ahn, A. Hariki, K.-W. Lee, and J. Kuneš, *Phys. Rev. B* **99**, 184432 (2019).
- [23] L.-D. Yuan, Z. Wang, J.-W. Luo, E. I. Rashba, and A. Zunger, *Phys. Rev. B* **102**, 014422 (2020).
- [24] X. Zhou, W. Feng, R.-W. Zhang, L. Šmejkal, J. Sinova, Y. Mokrousov, and Y. Yao, *Phys. Rev. Lett.* **132**, 056701 (2024).
- [25] L. Šmejkal, A. Marmodoro, K.-H. Ahn, R. González-Hernández, I. Turek, S. Mankovsky, H. Ebert, S. W. D'Souza, O. c. v. Šipr, J. Sinova, and T. c. v. Jungwirth, *Phys. Rev. Lett.* **131**, 256703 (2023).
- [26] Z. Feng, X. Zhou, L. Šmejkal, L. Wu, Z. Zhu, H. Guo, R. González-Hernández, X. Wang, H. Yan, P. Qin, X. Zhang, H. Wu, H. Chen, Z. Meng, L. Liu, Z. Xia, J. Sinova, T. Jungwirth, and Z. Liu, *Nature Electronics* **5**, 735 (2022).
- [27] Z. Lin, D. Chen, W. Lu, X. Liang, S. Feng, K. Yamagami, J. Osiecki, M. Leandersson, B. Thiagarajan, J. Liu, C. Felser, and J. Ma, *Observation of giant spin splitting and d-wave spin texture in room temperature altermagnet ruo2* (2024), arXiv:2402.04995 [cond-mat.mtrl-sci].
- [28] M. Hiraishi, H. Okabe, A. Koda, R. Kadono, T. Muroi, D. Hirai, and Z. Hiroi, *Phys. Rev. Lett.* **132**, 166702 (2024).
- [29] T. Berlijn, P. C. Snijders, O. Delaire, H.-D. Zhou, T. A. Maier, H.-B. Cao, S.-X. Chi, M. Matsuda, Y. Wang, M. R. Koehler, P. R. C. Kent, and H. H. Weitering, *Phys. Rev. Lett.* **118**, 077201 (2017).
- [30] Z. H. Zhu, J. Stremper, R. R. Rao, C. A. Occhialini, J. Pelliciani, Y. Choi, T. Kawaguchi, H. You, J. F. Mitchell, Y. Shao-Horn, and R. Comin, *Phys. Rev. Lett.* **122**, 017202 (2019).
- [31] A. Bose, N. J. Schreiber, R. Jain, D.-F. Shao, H. P. Nair, J. Sun, X. S. Zhang, D. A. Muller, E. Y. Tsymbal, D. G. Schlom, and D. C. Ralph, *Nature Electronics* **5**, 267 (2022).
- [32] Z. Q. Wang, Z. Q. Li, L. Sun, Z. Y. Zhang, K. He, H. Niu, J. Cheng, M. Yang, X. Yang, G. Chen, Z. Yuan, H. F. Ding, and B. F. Miao, *Phys. Rev. Lett.* **133**, 046701 (2024).
- [33] A. Smolyanyuk, I. I. Mazin, L. Garcia-Gassull, and R. Valentí, *Phys. Rev. B* **109**, 134424 (2024).
- [34] R. M. Fernandes, V. S. de Carvalho, T. Birol, and R. G. Pereira, *Phys. Rev. B* **109**, 024404 (2024).
- [35] C. R. W. Steward, R. M. Fernandes, and J. Schmalian, *Phys. Rev. B* **108**, 144418 (2023).

- [36] M. Naka, Y. Motome, and H. Seo, *Phys. Rev. B* **103**, 125114 (2021).
- [37] S. López-Moreno, A. H. Romero, J. Mejía-López, A. Muñoz, and I. V. Roshchin, *Phys. Rev. B* **85**, 134110 (2012).
- [38] S. López-Moreno, A. H. Romero, J. Mejía-López, and A. Muñoz, *Phys. Chem. Chem. Phys.* **18**, 33250 (2016).
- [39] Y. Noda, K. Ohno, and S. Nakamura, *Phys. Chem. Chem. Phys.* **18**, 13294 (2016).
- [40] S. A. Egorov, D. B. Litvin, and R. A. Evarestov, *The Journal of Physical Chemistry C* **125**, 16147 (2021).
- [41] P. E. Blöchl, *Phys. Rev. B* **50**, 17953 (1994).
- [42] T. Okugawa, K. Ohno, Y. Noda, and S. Nakamura, *Journal of Physics: Condensed Matter* **30**, 075502 (2018).
- [43] T. Urata, W. Hattori, and H. Ikuta, *Phys. Rev. Mater.* **8**, 084412 (2024).
- [44] S. Reimers, L. Odenbreit, L. Šmejkal, V. N. Strocov, P. Constantinou, A. B. Hellenes, R. Jaeschke Ubierno, W. H. Campos, V. K. Bharadwaj, A. Chakraborty, T. Denneulin, W. Shi, R. E. Dunin-Borkowski, S. Das, M. Kläui, J. Sinova, and M. Jourdan, *Nature Communications* **15**, 2116 (2024).
- [45] Y. Wu, L. Deng, X. Yin, J. Tong, F. Tian, and X. Zhang, *Nano Letters* **24**, 10534 (2024), pMID: 39145607.
- [46] M. Milivojević, M. Orozović, S. Picozzi, M. Gmitra, and S. Stavičić, *2D Materials* **11**, 035025 (2024).
- [47] T. Osumi, S. Souma, T. Aoyama, K. Yamauchi, A. Honma, K. Nakayama, T. Takahashi, K. Ohgushi, and T. Sato, *Phys. Rev. B* **109**, 115102 (2024).
- [48] I. I. Mazin, *Phys. Rev. B* **107**, L100418 (2023).
- [49] J. Krempaský, L. Šmejkal, S. W. D'Souza, M. Hajaoui, G. Springholz, K. Uhlířová, F. Alarab, P. C. Constantinou, V. Strocov, D. Usanov, W. R. Pudelko, R. González-Hernández, A. Birk Hellenes, Z. Jansa, H. Reichlová, Z. Šobáň, R. D. Gonzalez Betancourt, P. Wadley, J. Sinova, D. Kriegner, J. Minár, J. H. Dil, and T. Jungwirth, *Nature* **626**, 517 (2024).
- [50] S. Lee, S. Lee, S. Jung, J. Jung, D. Kim, Y. Lee, B. Seok, J. Kim, B. G. Park, L. Šmejkal, C.-J. Kang, and C. Kim, *Phys. Rev. Lett.* **132**, 036702 (2024).
- [51] A. Hariki, A. Dal Din, O. J. Amin, T. Yamaguchi, A. Badura, D. Kriegner, K. W. Edmonds, R. P. Campion, P. Wadley, D. Backes, L. S. I. Veiga, S. S. Dhesi, G. Springholz, L. Šmejkal, K. Výborný, T. Jungwirth, and J. Kuneš, *Phys. Rev. Lett.* **132**, 176701 (2024).
- [52] L.-D. Yuan, Z. Wang, J.-W. Luo, and A. Zunger, *Phys. Rev. Mater.* **5**, 014409 (2021).
- [53] S. Hayami, Y. Yanagi, and H. Kusunose, *Phys. Rev. B* **102**, 144441 (2020).
- [54] Y.-P. Zhu, X. Chen, X.-R. Liu, Y. Liu, P. Liu, H. Zha, G. Qu, C. Hong, J. Li, Z. Jiang, X.-M. Ma, Y.-J. Hao, M.-Y. Zhu, W. Liu, M. Zeng, S. Jayaram, M. Lenger, J. Ding, S. Mo, K. Tanaka, M. Arita, Z. Liu, M. Ye, D. Shen, J. Wrachtrup, Y. Huang, R.-H. He, S. Qiao, Q. Liu, and C. Liu, *Nature* **626**, 523 (2024).
- [55] L. Šmejkal, J. Sinova, and T. Jungwirth, *Phys. Rev. X* **12**, 040501 (2022).
- [56] G. A. Slack, *Phys. Rev.* **122**, 1451 (1961).
- [57] M. E. Lines, *Phys. Rev.* **137**, A982 (1965).
- [58] J. P. Van Der Ziel and H. J. Guggenheim, *Phys. Rev.* **166**, 479 (1968).
- [59] A. Ishikawa and T. Moriya, *Journal of the Physical Society of Japan* **30**, 117 (1971).
- [60] S. J. Allen and H. J. Guggenheim, *Journal of Applied Physics* **42**, 1657 (1971).
- [61] A. S. Disa, M. Fechner, T. F. Nova, B. Liu, M. Först, D. Prabhakaran, P. G. Radaelli, and A. Cavalleri, *Nature Physics* **16**, 937 (2020).
- [62] J. A. Barreda-Argüeso, S. López-Moreno, M. N. Sanz-Ortiz, F. Aguado, R. Valiente, J. González, F. Rodríguez, A. H. Romero, A. Muñoz, L. Nataf, and F. Baudelet, *Phys. Rev. B* **88**, 214108 (2013).
- [63] R. González-Hernández, L. Šmejkal, K. Výborný, Y. Yahagi, J. Sinova, T. c. v. Jungwirth, and J. Železný, *Phys. Rev. Lett.* **126**, 127701 (2021).
- [64] L. Šmejkal, A. B. Hellenes, R. González-Hernández, J. Sinova, and T. Jungwirth, *Phys. Rev. X* **12**, 011028 (2022).
- [65] D.-F. Shao, S.-H. Zhang, M. Li, C.-B. Eom, and E. Y. Tsymbal, *Nature Communications* **12**, 7061 (2021).
- [66] H. Bai, L. Han, X. Y. Feng, Y. J. Zhou, R. X. Su, Q. Wang, L. Y. Liao, W. X. Zhu, X. Z. Chen, F. Pan, X. L. Fan, and C. Song, *Phys. Rev. Lett.* **128**, 197202 (2022).
- [67] M. Naka, S. Hayami, H. Kusunose, Y. Yanagi, Y. Motome, and H. Seo, *Nature Communications* **10**, 4305 (2019).
- [68] R. He, D. Wang, N. Luo, J. Zeng, K.-Q. Chen, and L.-M. Tang, *Phys. Rev. Lett.* **130**, 046401 (2023).
- [69] G. Kresse and J. Hafner, *Phys. Rev. B* **47**, 558 (1993).
- [70] J. P. Perdew, K. Burke, and M. Ernzerhof, *Phys. Rev. Lett.* **77**, 3865 (1996).
- [71] J. P. Perdew, A. Ruzsinszky, G. I. Csonka, O. A. Vydrov, G. E. Scuseria, L. A. Constantin, X. Zhou, and K. Burke, *Phys. Rev. Lett.* **100**, 136406 (2008).
- [72] H. J. Monkhorst and J. D. Pack, *Phys. Rev. B* **13**, 5188 (1976).
- [73] S. L. Dudarev, G. A. Botton, S. Y. Savrasov, C. J. Humphreys, and A. P. Sutton, *Phys. Rev. B* **57**, 1505 (1998).
- [74] Y. Guo, H. Liu, O. Janson, I. C. Fulga, J. van den Brink, and J. I. Facio, *Materials Today Physics* **32**, 100991 (2023).
- [75] D. Litvin and W. Opechowski, *Physica* **76**, 538 (1974).
- [76] D. B. Litvin, *Acta Crystallographica Section A* **33**, 279 (1977).
- [77] J. Heyd, G. E. Scuseria, and M. Ernzerhof, *The Journal of Chemical Physics* **118**, 8207 (2003).
- [78] T. Ozawa and B. Mera, *Phys. Rev. B* **104**, 045103 (2021).
- [79] H. Lang, S. Zhang, and Z. Liu, *Phys. Rev. B* **94**, 235306 (2016).